

# VLBI System (BLK I) IF-Video Down Conversion Design

N. C. Ham

Telecommunications Systems Section

*The prototype IF-video down converter of the DSN BLK I VLBI system, a hybrid of analog and digital circuits, has been completed and tested. The initial results have met all design specifications, establishing a milestone in new design technology for such devices. This device has uses in other similar applications and can form the basis for expanded design and applications.*

## I. Introduction

The IF-video down converter is an assembly of the Deep Space Communication Complex (DSCC) BLK I Very Long Baseline Interferometry (VLBI) system which down converts the receiver intermediate frequency (IF) spectrum to video-band frequencies. The video-band spectrum, in digitized form, is then stored on high-capacity magnetic discs and simultaneously transmitted via wideband data lines (WBDL) from the DSCC to the VLBI Processing Center at the Jet Propulsion Laboratory (JPL) in near-time for further processing with similar data from other DSN complexes. The VLBI signal can be either an extragalactic radio source (ERS) or a spacecraft line-spectra signal (Ref. 1).

A fundamental problem in down converting a radio frequency (RF) and IF spectrum to the lower video-band frequencies is that of suppressing the image (or adjacent band) noise which would cause signal-to-noise ratio (SNR) degradation to the received signal spectrum.

Similarly, in the conversion, the signal phase information in the video output data must not have been subjected to phase instabilities and fluctuations. This is an essential requirement when the system is used to accurately determine the group delay of a limited span bandwidth spacecraft radiated signal during a delta differenced one-way range ( $\Delta$ DOR)

observation. The alternate observation of a spacecraft and ERS signal during  $\Delta$ DOR aids in the navigation of the spacecraft into deep space.

A prototype down-converter assembly, comprised of hybrid analog and digital circuits, has been designed, constructed and tested and meets the specified system requirements for image-band rejection and limited SNR degradation.

Other important specifications met were the capability for down converting narrow segment bandwidths of the wide bandwidth RF S- and X-band spectra through separate wide-band RF channels, providing a dynamic signal amplitude reception range, selectable channel output bandwidths, and low imparted phase instabilities and fluctuations.

The design specifications, including error budgets and element contribution limits, that form part of the overall VLBI system design are listed in Table 1.

## II. Design Configuration and Rationale

The basic design of the down-converter is an extension of an existing all-analog design which has been used for this application and achieves the image spectrum rejection by utilizing a phase quadrature cancellation technique (Ref. 1).

Figure 1 is the block diagram of the converter and labels the analog and digital portions. Major components are the analog IF mixer, local oscillators and selector, video amplifiers and anti-aliasing filters, and digital input signal multiplexer, analog-to-digital converter (ADC), 90° phase shifter, combiner, low-pass filters, decimator and formatter, and computer interface for control and operation.

The hybrid design exploits the advantages of both circuit domains for meeting the design requirements. For example, the analog circuits are best applicable at the IF range from 265 to 400 MHz for achieving the IF-LO conversion to video band and in maintaining the quadrature phase for less than an octave range.

The implementation of the second quadrature phase shift over a 5-octave range while maintaining low-phase variation (ripple) was achieved in the digital domain. Similarly, the low-pass filters, decimator, and formatter are better achieved in this domain and in ensuring the success for overall repeatable characteristics and reproduction.

Two IF-video converters (analog portion) are used for the S- and X-band spectra to break the frequency ratio into lesser ranges of 265 to 305 MHz and 300 to 400 MHz, respectively, to aid in maintaining the quadrature phase, and video signal amplitude match. Lumped circuit hybrids were used to obtain the quadrature phase shift at these local oscillator frequencies (Ref. 2).

Eight frequency synthesizers are available for the X-band spectrum and four for the S-band spectrum down conversion. Figure 2 illustrates a typical spacecraft spectrum such as will be transmitted by the Galileo spacecraft during a  $\Delta$ DOR observation. The two extreme sideband tones (X-band) are used to determine the signal group delay, while the close-in side tones and carrier signals are used to resolve the delay ambiguity in determining the outermost sideband tone phases. This is necessary when using several narrow bandwidth channels to determine the broader bandwidth signal group delay and is known as bandwidth synthesis (BWS) (Ref. 3).

The individual frequency synthesizers are tuned to align with the appropriate sidebands (S- and X-band spectra) which are sequentially time multiplexed in a cyclic manner to obtain their phase. Each oscillator is left operating at its tuned frequency during the multiplexing procedure to maintain continuity of the signal phase. A typical multiplexed sequence is shown in Fig. 3 for both the spacecraft signal and the alternate ERS spectrum (at approximately the same channel frequency) during a  $\Delta$ DOR observation.

Only the ERS spectrum is observed when the system is used for obtaining VLBI data for time synchronization and Earth motion precision observations, and the system will utilize the full bandwidth of the S- and X-band IF spectra and the frequency synthesizers tuning capability.

For the digital portion, the two quadrature video-band signals from the mixers (Fig. 1) are input to the analog-to-digital converter for digitization. The two digitized signals are then input to the phase shifter for shifting the video spectrum of one signal an additional 90 degrees relative to the other. The phase shifter design is based on a 90° phase-shifting network using the Jacobian elliptic function together with the bilinear transform.

A pair of all-pass networks was derived whose phase difference was the closest approximation to 90° over the range of video-band frequencies. A total of 6 poles and zeros was used to achieve the desired response.

The digital low-pass filter design was adopted from an existing computer program (Ref. 4) for elliptic filters.

The hybrid converter design differs in another major way from previous all-analog designs in that the signal amplitude linearity must be maintained throughout the complete signal path (including digitization and digital processing) until the low-pass filtering is accomplished. Digitally this prevents register overflow and preserves the computation integrity during the video-band phase shift, image-band rejection and low-pass filtering process. Following this processing, the signal is reduced in data volume by sequential data selection (decimated, the selection rate is reducible to 1/16 in 1/2 increments). The reduced data rate coincides with the selected low-pass filter bandwidth while preserving the Nyquist criterion. Finally, the data are formatted into a 1-bit quantization as the data form. The amplitude differences in the carrier and sideband tones (shown in Fig. 2) together with the necessity for linearity define one requirement for the dynamic range of the ADC. Another requirement is to accommodate the amplitude difference between the spacecraft and ERS signals as the observation alternates between these two signals sources.

Although the dynamic range of the ADC was adequate to accommodate the amplitude differences of the above signals during a given observation period, it is not adequate (nor was it considered necessary) to handle the extremes of the received spacecraft signal level throughout the entire mission-time profile. Figure 4 illustrates the anticipated signal power-time profile for the Galileo mission.

Since the power level extremes occur over many days and the ADC dynamic range can accommodate the expected range during segments of this profile, a computer-controlled attenuator at the IF amplifier output prior to the input of the frequency down-converter can be preset during any observation day to optimize the expected signal level range to the ADC characteristics. This is applicable to either the line-spectra spacecraft or ERS continuous-spectra signals during either a  $\Delta$ DOR or time and Earth-motion observations (Ref. 2).

### III. Design Detail and Error Budget

There were subtle design details that were confronted in meeting the overall requirements, such as the technical management to allow subassemblies to be designed and developed with individual specification using independent and separate schedules, personnel, and laboratories.

The requirements were critically specified, top down from the system requirements, using engineering judgment towards the error budget allocation with the apportionment balanced on the state-of-the-art design and components technology, complexity, and ease of duplication. Budget allocation was reassessed and trade-offs made during the development with the greatest tolerance value rebudgeted to the most difficult circuit domain.

A typical example is the specification of parameters that affected the image rejection and phase variation. The parameter error sensitivity was formulated and provided the basis for distributing the budget allocation.

For example, from the diagram of Fig. 1 the equation for the top mixer and video amplifier string signal can be written as,

$$V_{TO} = V_S [\cos(\omega_S \rightarrow \omega_{US})t + \cos(\omega_S \rightarrow \omega_{LS})t] \quad (1)$$

(Note that  $\omega_S \rightarrow \omega_{US}$  indicates the range of frequencies from  $\omega_S$  to  $\omega_{US}$  [Ref. 1].) The bottom string can be written as,

$$V_{BO} = (V_S + \delta) [\sin(\omega_S \rightarrow \omega_{US})t + \phi_A - \sin(\omega_S \rightarrow \omega_{LS})t + \phi_A] \quad (2)$$

where  $(\omega_S \rightarrow \omega_{LS})$  is the lower spectrum band from the signal frequency  $\omega_S$  and  $(\omega_S \rightarrow \omega_{US})$  is the upper spectrum. The frequency  $\omega_S$  is also the edge of the desired down-converted spectrum and is equal to the local oscillator signal  $\omega_{LO}$  (Ref. 1).  $\delta_A$  and  $\phi_A$  are the amplitude (from equal value) and phase (from 90 degrees difference) errors of the two analog output signals. Small error values or near-perfect amplitude

and quadrature phase tracking implies near-infinite image-band suppression.

Following digitization, the upper signal is shifted an additional  $90^\circ$  relative to the lower signal,

$$V_{TO}'' = V_S'' [\sin(0 \rightarrow \omega_{US})t + \phi_D + \sin(0 \rightarrow \omega_{LS})t + \phi_D] \quad (3)$$

where  $V_S''$  is the new amplitude from the ADC. Sin 0 represents the zero frequency or dc component since  $\omega_S = \omega_{LO}$ , and  $\phi_D$  is the error of the digital  $90^\circ$  phase shifter in producing a true quadrature phase to all frequencies across  $0 \rightarrow \omega_{US}$  and  $0 \rightarrow \omega_{LS}$ .

Similarly, the bottom signal input to the combiner is,

$$V_{BO}'' = (V_S + \delta)'' [\sin(0 \rightarrow \omega_{US})t + \phi_A - [\sin(0 \rightarrow \omega_{LS})t + \phi_A]] \quad (4)$$

The combiner sums the two input signals, expressed by Eqs. (3) and (4) and cancels the lower sideband or image spectrum and obtains the desired passband spectrum as follows:

$$V_{CANCEL} = V_S'' [\sin(0 \rightarrow \omega_{LS})t + \phi_D - (V_S + \delta) [\sin(0 \rightarrow \omega_{LS})t + \phi_A]] \quad (5)$$

$$V_{OUT} = V_S'' [\sin(0 \rightarrow \omega_{US})t + \phi_D + \sin(0 \rightarrow \omega_{US})t + \phi_A] \quad (6)$$

The vector diagram of Fig. 5 illustrates the upper and lower spectra signals relative to Eqs. (1) through (6). From the combiner summed output diagrams of Fig. 5(c) and (d) showing the desired passband and reject band signals, an equation for the image rejection magnitude can be derived.

The passband signal amplitude is

$$V_{PASS} = \left\{ [(V_U + \delta) + (V_U \cos \sigma)]^2 + (V_U \sin \sigma)^2 \right\}^{1/2} \quad (7)$$

and the reject band signal amplitude is

$$V_{REJECT} = \left\{ [(V_L + \delta) - (V_L \cos \sigma)]^2 + (V_L \sin \sigma)^2 \right\}^{1/2} \quad (8)$$

The image spectrum rejection magnitude is the ratio of the passband spectrum, amplitude relative to the image spectrum amplitude, and expressed in dB becomes,

$$\text{I.R.} = 10 \log \frac{2(1 + \delta)(1 + \cos \sigma) + \delta^2}{2(1 + \delta)(1 - \cos \sigma) + \delta^2} \quad (9)$$

where  $\delta$  is the amplitude difference between the two video-band signals prior to the combining;  $\delta = V'_{BO} - V'_{TO}$ ; and  $\sigma$  is the net phase error from  $90^\circ$ .

The design error budget for the analog portion of the converter was set to  $90^\circ \pm 4^\circ$  and  $\pm 0.4$  dB in quadrature phase and amplitude imbalance, respectively, for the two video-output signals over any 600 kHz segment bandwidth within the S- and X-band IF range.

These error contributions would insure an image rejection to a value

$$\text{I.R. (analog)} = 10 \log \frac{2(1.05)(1 + 0.99756) + 0.05^2}{2(1.05)(1 - 0.99756) + 0.05^2}$$

or

$$\text{I. R.} = 27.4 \text{ dB}$$

For the digital portion, a value of  $90^\circ \pm 0.75^\circ$  was specified. The  $\pm 0.75^\circ$  error includes the phase ripple parameter across the passband range which is largely contributed to by the all-pass  $90^\circ$  phase-shift network.

The error budget of  $\leq 1^\circ$  peak-phase variation (ripple) is important when the spacecraft line-spectra signal is to be received during a  $\Delta$ DOR observation. With a maximum sideband tone separation of 38 MHz, the contribution of  $1^\circ$  peak-phase error could result in an error of 1 cm in the signal group delay determination (Ref. 1). The phase error is manifest in the determination of the line-spectra sideband signal phase when it lies in between calibration tones during the reception-data-acquisition process.

The calibration tones are injected as a comb (equally spaced in frequency) of phase-stable tones into the VLBI system microwave input to aid in calibrating out the system-incurred phase variations during the final data processing. The phase of a fixed-frequency spacecraft signal falling in between the calibration tones would be difficult to determine should a large phase ripple exist. The error specification placed a limit on the resultant error contributed by the ripple between any two phase calibration tones. As will be discussed later in the test data, the measured ripple was better than specified and resulted in a linear interpolation factor.

Other contributors to the amplitude SNR degradation are the aliasing, quantization, and noise spectral density. The ADC

largely contributed the noise spectral density and quantization noise, which, with the need for  $\geq 48$  dB signal amplitude dynamic range, imposed the requirement for a quality ADC.

A 15-bit, state-of-the-art, ADC manufactured by Preston Scientific (Model GMAD-1A) is used and contains an equivalent noise spectral density (noise floor) of 0.75 millivolts rms.

The ADC has a  $\pm 5$ -V peak-volts signal input capability. Relative to this the  $2^8$ -bit level minimum resolvable signal voltage of 19.5 mV results in a 48 dB dynamic capability.

The noise floor value, relative to 19.5 mV, results in a value 28 dB below this minimum signal and meets this error specification.

For quantization noise the equation is

$$Q_{\text{Noise}} = \frac{Q}{2\sqrt{3}} = \frac{\text{Full Scale Range}}{2^n 2/\sqrt{3}}$$

where  $Q$  is the quantum (or quantization size) and  $2/\sqrt{3}$  is the conversion of the sampling residual triangular waveform to rms volts. Thus, the quantization voltage relative to the 5 V full-scale range is

$$\begin{aligned} V_{\text{Quant}} &= \frac{5}{2^{15} \times 1.15} \\ &= 0.13 \text{ mV rms} \end{aligned}$$

and relative to the minimum resolvable signal level of 19.5 mV, the quantization noise is,

$$\begin{aligned} Q_{\text{Noise}} &= 20 \log \frac{19.5}{0.1327} \\ &= 43 \text{ dB} \end{aligned}$$

and meets this error budget.

Aliasing noise is reduced by the shape characteristics of the anti-aliasing filter following the analog amplifiers relative to the sampling frequency of the ADC. Figure 6 illustrates the filter response, sampling frequency, and resultant aliasing noise response, and shows that the lower sampled sideband and data passband overlapping regions are  $> 73$  dB below the passband spectrum. Thus aliasing noise meets the specified budget value of  $\geq 25$  dB even when the signal is 48 dB below the 5-V maximum ADC input.

## IV. Test Results

The initial test results from the prototype unit met all design specifications. Individual tests on the analog portion were performed first because of its development schedule and were later combined with the digital portion as the latter was designed and constructed for the overall tests.

Table 2 tabulates the amplitude and quadrature phase tracking of the analog IF-VF mixer over the frequency range from 265 to 400 MHz. Measurements were at frequencies of 265, 300, 325, 350, 375, and 400 MHz where the input signal was stepped across a 10 to 300 kHz band at each of these frequencies.

Figures 7 and 8, for the 250 kHz and 125 kHz LPF bandwidth, are the test results of the complete IF-video converter amplitude response over a  $\pm 300$  kHz spectrum about a local oscillator frequency of 300 MHz.

These two responses are typical for all the low-pass filter (LPF) bandwidths for any segment within the total IF spectrum. The results indicate that the analog and digital circuits tend to compensate the imbalance across the bandwidth and result in an image rejection greater than 34 dB.

The input signal for these results was set to the maximum value of the ADC at  $\pm 5$  V. When the signal levels were lowered to input values of  $\pm 0.5$  V and  $\pm 0.05$  V into the ADC, the amplitude response had similar characteristics, indicating that the image rejection and passband characteristics would be preserved with a minimum signal 48 dB below the maximum signal capability. This range meets the dynamic range specification.

Figure 9 compares the expected phase shift versus frequency (calculated from the filter design) against the measured phase of the prototype unit and indicates close agreement.

Figure 10 is the design phase-ripple response versus frequency of the all-pass  $90^\circ$  digital phase shifter.

To determine the amount of phase ripple present in the total IF-video converter response shown in Fig. 9, a smoothing program was used to obtain an average phase versus frequency response for the measured data. The difference between the actual data and the average response was derived and plotted as shown in Fig. 11 for the 250 kHz LPF. This figure illustrates the nature of the ripple and indicates that the difference is less than a  $\pm 1^\circ$  peak between 40 kHz to 205 kHz and within these frequency limits meets the specification relative to an average response. The nearly symmetrical variation of the phase ripple about the average response would imply that the

phase response could be modeled between any 50 kHz segment band. This would aid in the operational utilization since some interpolation factor between any 50 kHz calibration tone could be adopted.

Figures 12, 13, 14, and 15 are such comparisons between the measured value and a linear regression analysis over a 50 kHz segment beginning from 10 kHz to 60 kHz and so on. For example, Fig. 13 is for the frequency segments from 60 to 110 kHz and 80 to 130 kHz and shows the linear curve comparison versus the data points. The correlation coefficient is 1.000, and resultant residuals are averaging below  $\pm 1^\circ$ .

The remaining plots for other segment frequency ranges indicate low residual values except for the two end segments, i.e., 10 kHz to 80 kHz and 160 kHz to 230 kHz.

These results are acceptable since the tuning resolution of the digitally tuned frequency synthesizers (IF-video converter local oscillators) can place the spacecraft signal near the center of the LPF passband. Similarly, since the residuals are well within the  $1^\circ$  peak limit near the passband center region, the phase value between the 50 kHz calibration tones can be linearly interpolated to limit expected errors to well within the total overall system error allocation. There is no reason that the linear phase range could not be extended should such a requirement be necessary for other applications.

## V. Summary

The requirements for good image-band rejection and low-phase variation IF-video converters was dictated by spacecraft navigation application. These were necessary because of the low-flux densities of available extragalactic radio sources that will be viewed near the spacecraft trajectory and the nature of accurately determining the phase information of the spacecraft line-spectra type signal having low-span bandwidth.

Assemblies of the DSCC BLK I VLBI system have been developed and tested which met these stringent requirements using a hybrid of analog and digital circuits. The performance has exceeded the characteristics of existing analog converters presently being used for similar VLBI applications.

The use of this converter design is not restricted to VLBI uses. It has application wherever a radio frequency spectrum must be down-converted to video-band frequencies for detection, data recording, or transmission over moderate bandwidth transmission circuits with tuning flexibility covering a broad spectrum.

Typical of such application is the observation and analysis of spacecraft carrier signals during planet occultation, orbiting satellite signals, and signal detection over an extremely broad spectrum such as the Search for Extra Terrestrial Intelligence (SETI).

Good amplitude and quadrature phase matching over a wide range of IF were achieved with analog circuits while low

phase variation all-pass phase shifters and realizable low-pass filters were accomplished using digital circuits.

The digital circuits following ADC will always cover a common range of video-band frequencies, regardless of the RF and IF range. This simplifies the circuit design to few functional types and lends itself to Very Large Scale Integration (VLSI) modules.

## Acknowledgment

I wish to acknowledge the contributions of V. M. Chavez, V. S. Chen, and T. Sato for the design, development, and testing of the IF video converter.

## References

1. Ham, N. C., "Frequency Down-Converter as Applied to VLBI," *TDA Progress Report 42-53*, pp. 74-82, Jet Propulsion Laboratory, Pasadena, California, July 1979.
2. SOSA, E. N., et. al., "Narrow Channel Bandwidth Receiver for VLBI," *TDA Progress Report 42-64*, pp. 18-29, Jet Propulsion Laboratory, Pasadena, California, May 1981.
3. Molinder, J. I., "A Tutorial Introduction to Very Long Baseline Interferometry (VLBI) Using Bandwidth Synthesis," *TDA Progress Report 42-46*, pp. 16-28, Jet Propulsion Laboratory, Pasadena, California, May 1978.
4. Gray, A. H., Jr., Markel, J. D., "A Computer Program for Designing Digital Elliptic Filters," *IEEE Transaction on Acoustics, Speech and Signal Processing*, Vol. ASSP-24, No. 6, pp. 529-538, December 6, 1976.

**Table 1. Design specifications**

<b>RF-IF Spectra</b>	
X-band	8400-8500 MHz
S-band	2265-2305 MHz
IF <sub>x</sub>	300-400 MHz
IF <sub>s</sub>	265-305 MHz
<b>Output Channels</b>	
Number of channels (Time and Frequency Multiplexed)	8 for X-band 4 for S-band
Bandwidth Selection, kHz	250 125 62.5 31.25
Data Format	1-bit quantization
Signal Phase Continuity (During the time-frequency multiplexing)	Phase continuity of each chan- nel signal must be maintained over the length of the obser- vation period.
Signal Reception Amplitude Dynamic Range	≥ 48 dB, ratio of maximum to minimum signal resolved
Operational Control	Automatic control of all functions during operation
Functions:	Frequency tuning Channel multiplexing RF spectra selection Channel bandwidth
Signal Amplitude SNR Degradation	≤ 1%
<b>Error Budget Allocation</b>	
Image band rejection	≥ 23 dB below passband level
Aliasing noise	≥ 25 dB below minimum signal resolution
Quantization noise	≥ 25 dB below minimum signal resolution
Signal Phase SNR Degradation	≤ 1%
<b>Error Budget Allocation:</b>	
Dispersive phase error (random)	$\sigma_{\phi} < 1^{\circ}$ rms
Phase variation (nonrandom)	$\sigma_{\phi} 1^{\circ}$ peak

**Table 2. Test results of typical analog portion of IF video converter**

Oscillation Frequency	265 MHz		300 MHz		325 MHz		350 MHz		375 MHz		400 MHz	
Output Frequency kHz	$\Delta A$ , dB	$\Delta\phi$ , deg	$\Delta A$ , dB	$\Delta\phi$ , deg	$\Delta A$ , dB	$\Delta\phi$ , deg	$\Delta A$ , dB	$\Delta\phi$ , deg	$\Delta A$ , dB	$\Delta\phi$ , deg	$\Delta A$ , dB	$\Delta\phi$ , deg
10	0.5	0.1	0.5	-0.7	0.5	-0.8	0.6	0	0.6	-0.2	0.6	0
25	0.4	0.1	0.5	-0.6	0.5	-0.8	0.6	0	0.6	-0.1	0.7	0.1
50	0.4	0.2	0.5	-0.6	0.5	-0.8	0.5	0	0.6	-0.1	0.7	0.1
75	0.5	0.3	0.5	-0.6	0.5	-0.7	0.5	0.1	0.6	-0.1	0.7	0.1
100	0.5	0.3	0.5	-0.5	0.5	-0.7	0.5	0.1	0.6	-0.1	0.7	0.1
125	0.4	0.3	0.5	-0.5	0.5	-0.7	0.5	0.1	0.6	0	0.6	0.1
150	0.4	0.3	0.5	-0.5	0.5	-0.7	0.5	0.1	0.6	0	0.8	0.2
175	0.4	0.3	0.5	-0.5	0.4	-0.7	0.4	0.1	0.6	0	0.8	0.2
200	0.3	0.3	0.5	-0.5	0.4	-0.7	0.4	0.1	0.6	0	0.8	0.1
225	0.3	0.3	0.5	-0.6	0.4	-0.7	0.4	0.1	0.6	-0.1	0.8	0.1
250	0.3	0.2	0.4	-0.6	0.5	-0.8	0.5	0	0.5	-0.1	0.7	0.1
275	0.3	0.1	0.4	-0.7	0.5	-0.9	0.5	-0.1	0.6	-0.2	0.6	0
300	0.3	0.1	0.5	-0.7	0.4	-0.9	0.5	-0.1	0.6	-0.2	0.7	-0.1

Output frequency =  $F_{\text{INPUT}} - F_{\text{OSCILLATOR}}$

$\Delta A$  = Difference between two output video frequencies

$\Delta\phi$  = Difference from quadrature between output frequencies

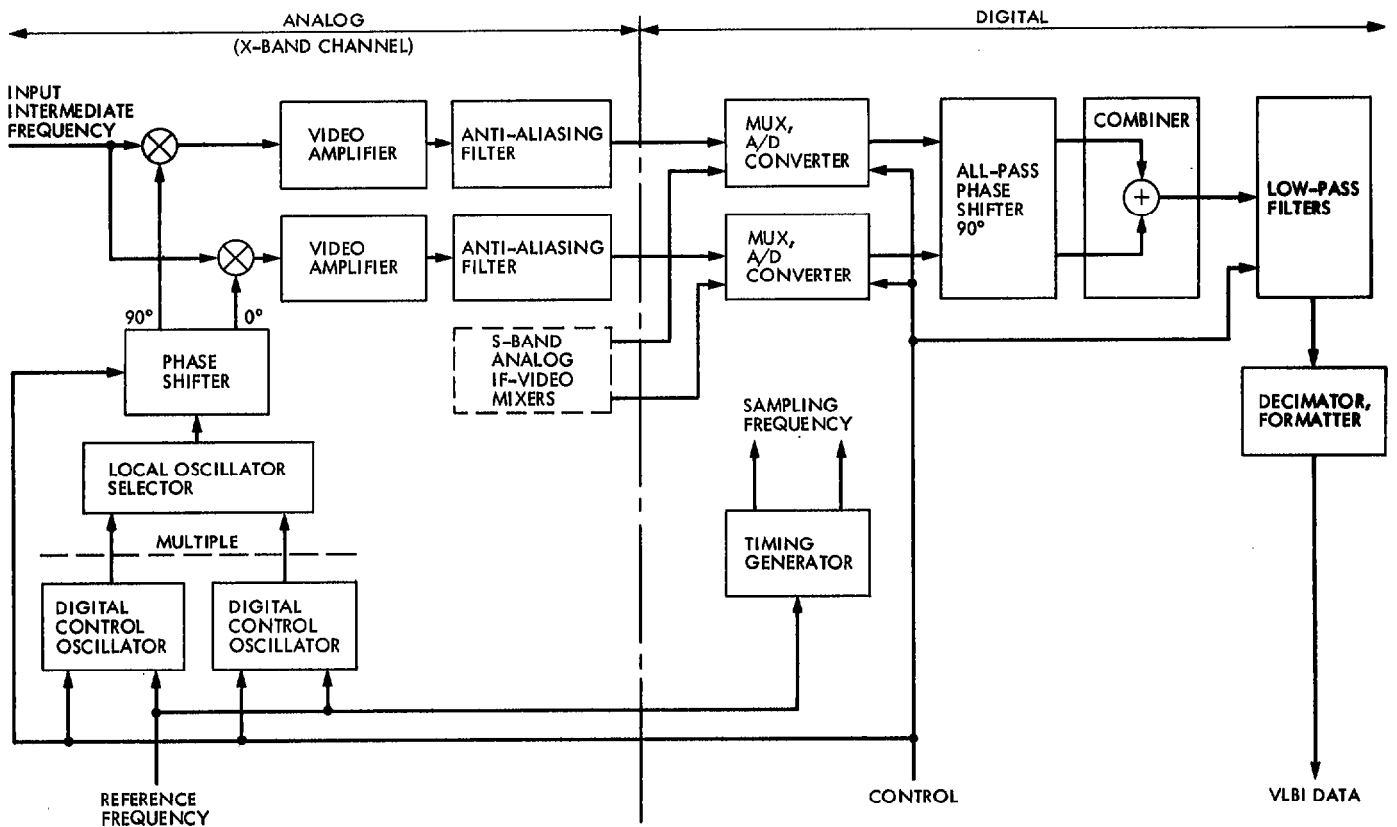


Fig. 1. IF-video converter

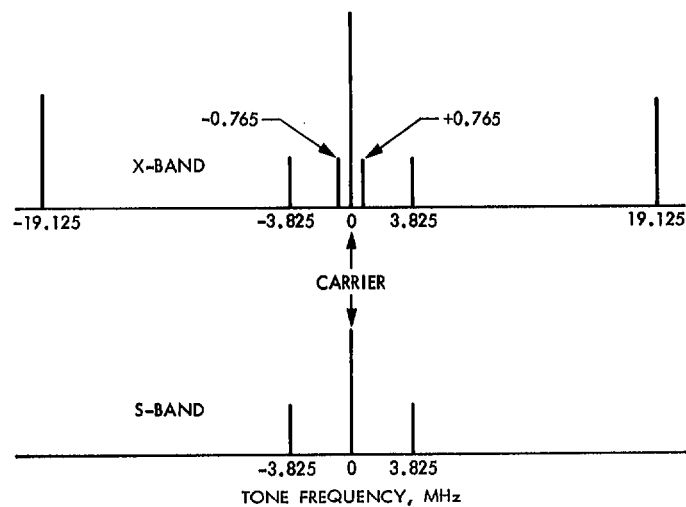


Fig. 2. Frequencies of the Galileo tones

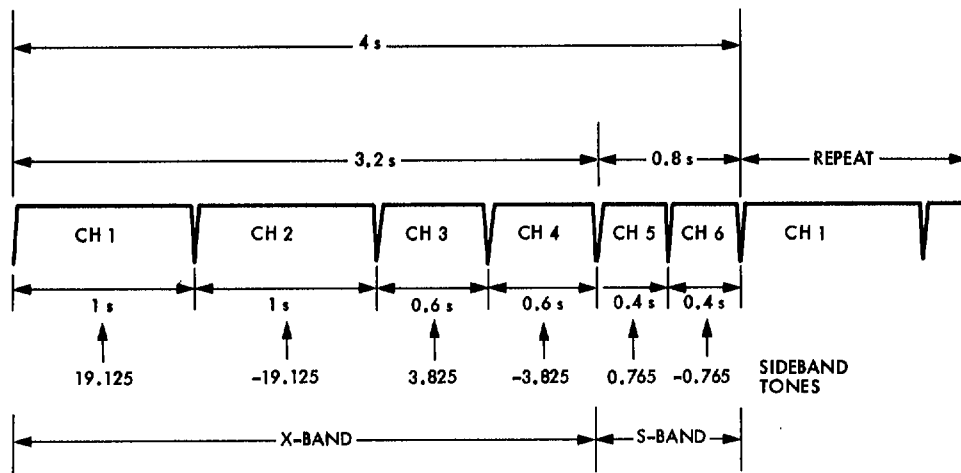


Fig. 3. Typical multiplexed channel sequence of spacecraft sideband tones

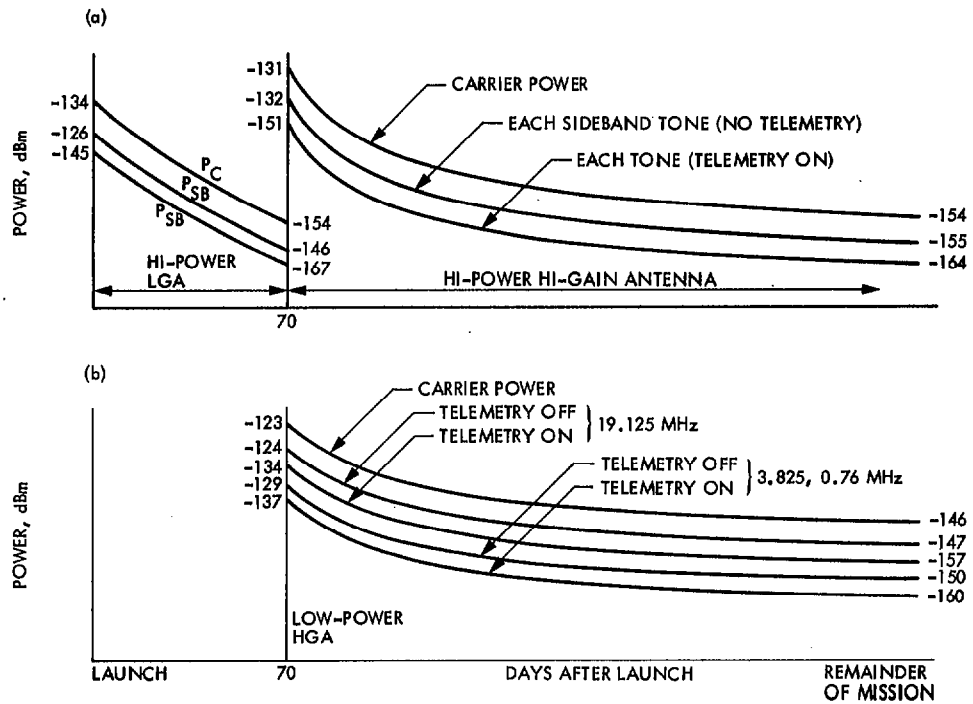


Fig. 4. Received spacecraft power level vs time profile: (a) S-band; (b) X-band

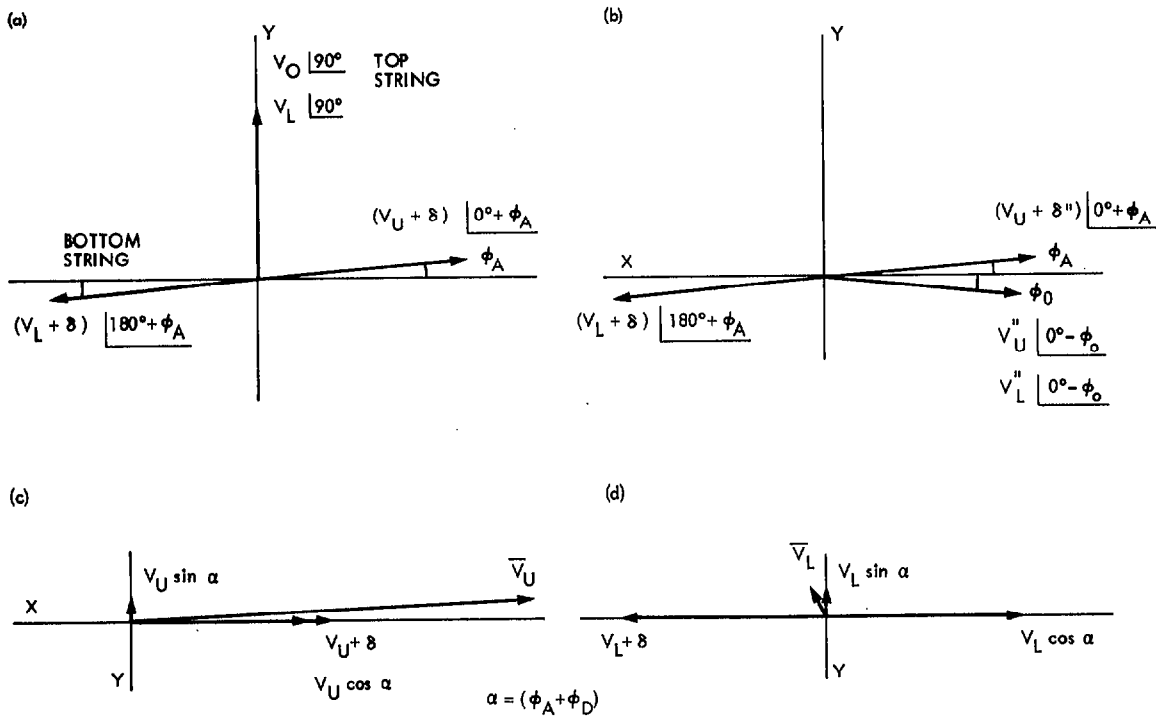


Fig. 5. Vector diagrams for upper- and lower-band spectrum: (a) video amplifiers output; (b) digital phase shifter output; (c) combiner summed output for desired passband upper-band spectrum; (d) combiner summed output for rejected image lower-band spectrum

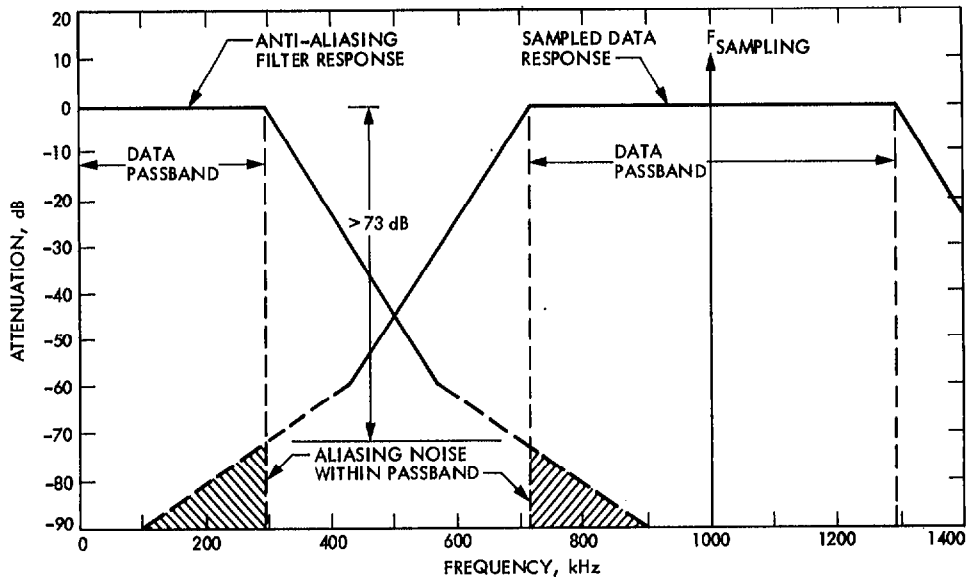


Fig. 6. Down converted video and sampled data spectra

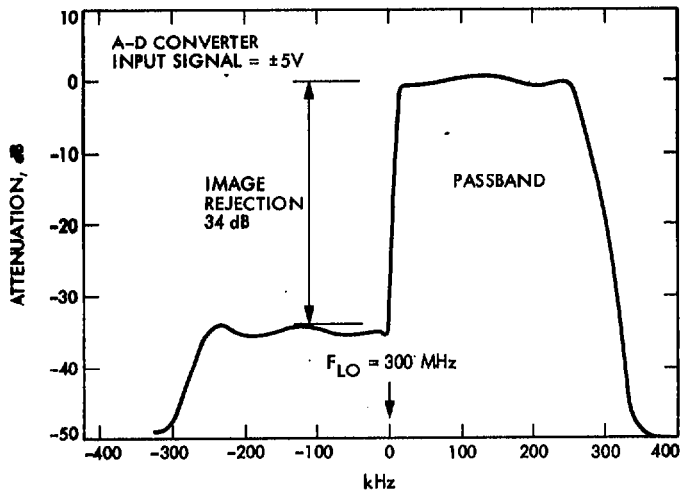


Fig. 7. Total response of IF-video converter for 250 kHz bandwidth

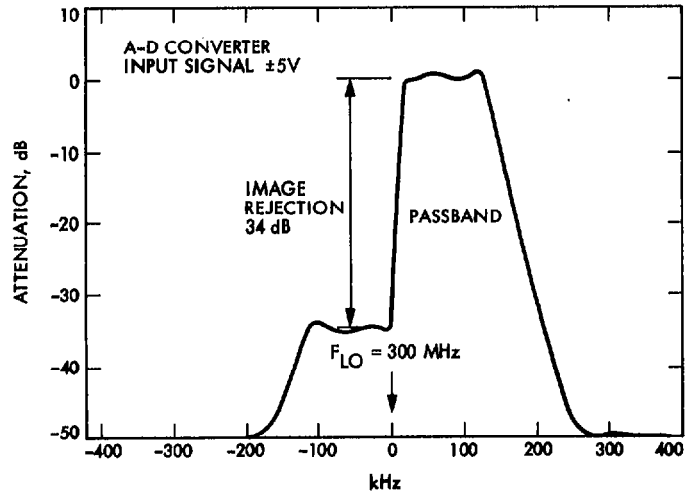


Fig. 8. Total response of IF-video converter for 125-kHz bandwidth

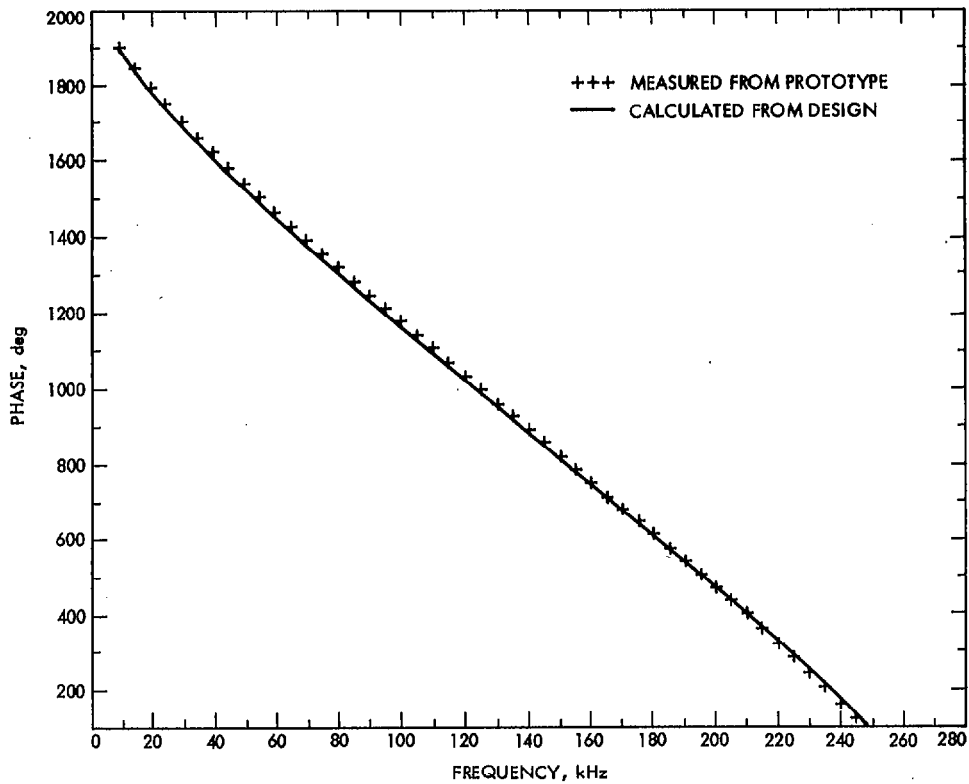


Fig. 9. Data channel filter, phase response (250 kHz BW)

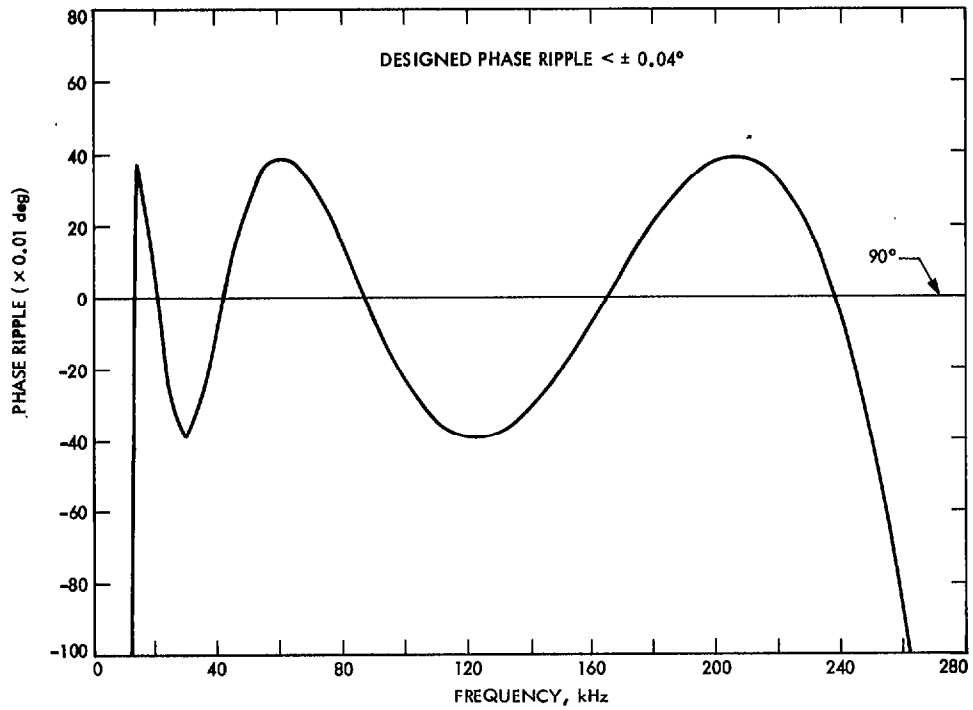


Fig. 10. Data channel filter, 90° phase shifter

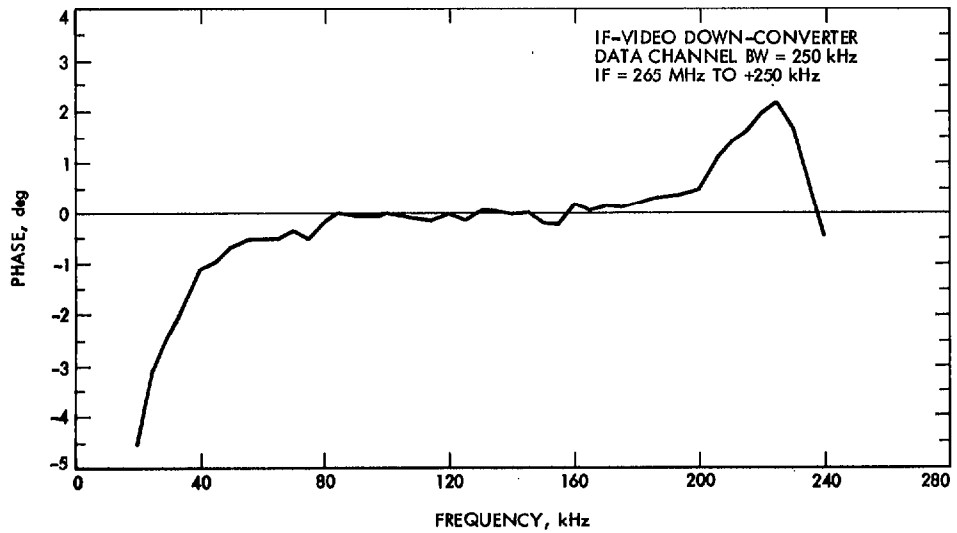


Fig. 11. Phase difference between actual and smoothed average phase response

R SQUARE = 0.997

YHAT = 2348.528 + -10.284 X

X(I)	Y(I)	YHAT	RESIDUALS
10.00	2265.70	2245.69	20.01
15.00	2198.70	2194.27	4.43
20.00	2138.40	2142.84	-4.44
25.00	2082.50	2091.42	-8.92
30.00	2029.50	2040.00	-10.50
35.00	1978.80	1988.58	-9.78
40.00	1930.10	1937.16	-7.06
45.00	1882.20	1885.74	-3.54
50.00	1835.50	1834.32	1.18
55.00	1789.30	1782.90	6.40
60.00	1743.70	1731.48	12.22

R SQUARE = 1.000

YHAT = 2300.653 + -9.240 X

X(I)	Y(I)	YHAT	RESIDUALS
30.00	2029.50	2023.46	6.04
35.00	1978.80	1977.27	1.53
40.00	1930.10	1931.07	-0.97
45.00	1882.20	1884.87	-2.67
50.00	1835.50	1838.67	-3.17
55.00	1789.30	1792.47	-3.17
60.00	1743.70	1746.27	-2.57
65.00	1698.50	1700.08	-1.58
70.00	1654.00	1653.88	0.12
75.00	1609.60	1607.68	1.92
80.00	1566.00	1561.48	4.52

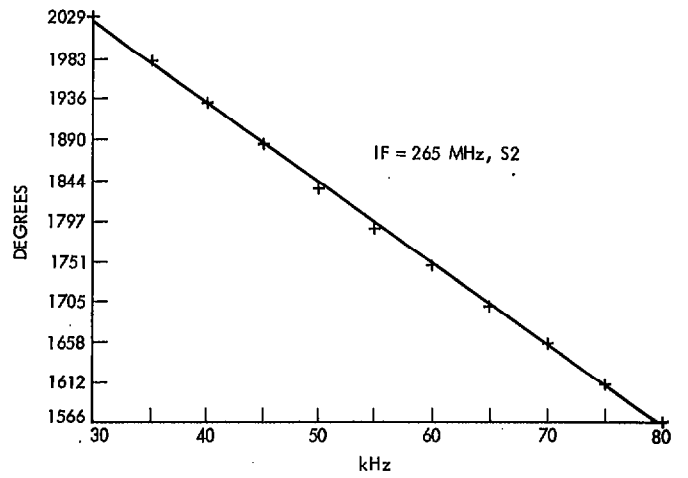
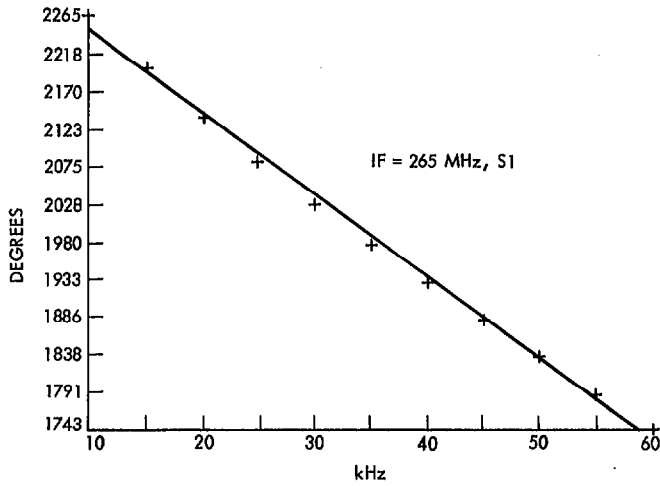


Fig. 12. Linear regression analysis results from 10 to 80 kHz

R SQUARE = 1.000

YHAT = 2266.979 + -8.751 X

X(I)	Y(I)	YHAT	RESIDUALS
60.00	1743.70	1741.91	1.79
65.00	1698.50	1698.16	0.34
70.00	1654.00	1654.40	-0.40
75.00	1609.60	1610.65	-1.05
80.00	1566.00	1566.89	-0.89
85.00	1522.50	1523.14	-0.64
90.00	1478.90	1479.38	-0.48
95.00	1435.40	1435.63	-0.23
100.00	1392.00	1391.87	0.13
105.00	1348.60	1348.11	0.49
110.00	1305.30	1304.36	0.94

R SQUARE = 1.000

YHAT = 2257.964 + -8.656 X

X(I)	Y(I)	YHAT	RESIDUALS
80.00	1566.00	1565.45	0.55
85.00	1522.50	1522.17	0.33
90.00	1478.90	1478.89	0.01
95.00	1435.40	1435.61	-0.21
100.00	1392.00	1392.33	-0.33
105.00	1348.60	1349.05	-0.45
110.00	1305.30	1305.76	-0.46
115.00	1262.10	1262.48	-0.38
120.00	1219.20	1219.20	-0.00
125.00	1176.10	1175.92	0.18
130.00	1133.40	1132.64	0.76

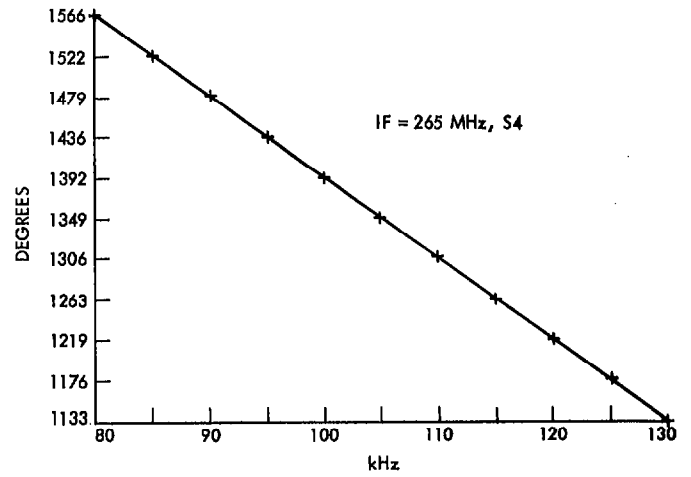
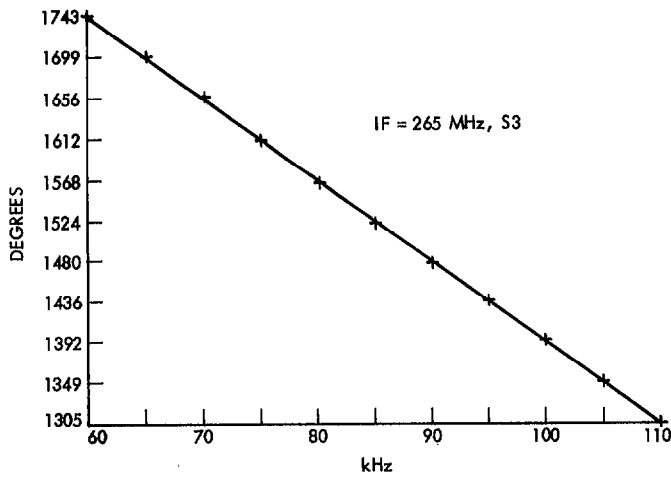


Fig. 13. Linear regression analysis results from 60 to 130 kHz

R SQUARE = 1.000  
 YHAT = 2248.161 + -8.575 X

X(I)	Y(I)	YHAT	RESIDUALS
110.00	1305.30	1304.94	0.36
115.00	1262.10	1262.07	0.03
120.00	1219.20	1219.19	0.01
125.00	1176.10	1176.32	-0.22
130.00	1133.40	1133.45	-0.05
135.00	1099.50	1090.57	-0.07
140.00	1047.50	1047.70	-0.20
145.00	1004.70	1004.83	-0.13
150.00	961.70	961.95	-0.25
155.00	919.00	919.08	-0.08
160.00	876.80	876.20	0.60

R SQUARE = 1.000  
 YHAT = 2243.333 + -8.541 X

X(I)	Y(I)	YHAT	RESIDUALS
130.00	1133.40	1132.99	0.41
135.00	1090.50	1090.29	0.21
140.00	1047.50	1047.58	-0.08
145.00	1004.70	1004.87	-0.17
150.00	961.70	962.17	-0.47
155.00	919.00	919.46	-0.46
160.00	876.80	876.76	0.04
165.00	834.10	834.05	0.05
170.00	791.60	791.35	0.25
175.00	748.80	748.64	0.16
180.00	706.00	705.94	0.06

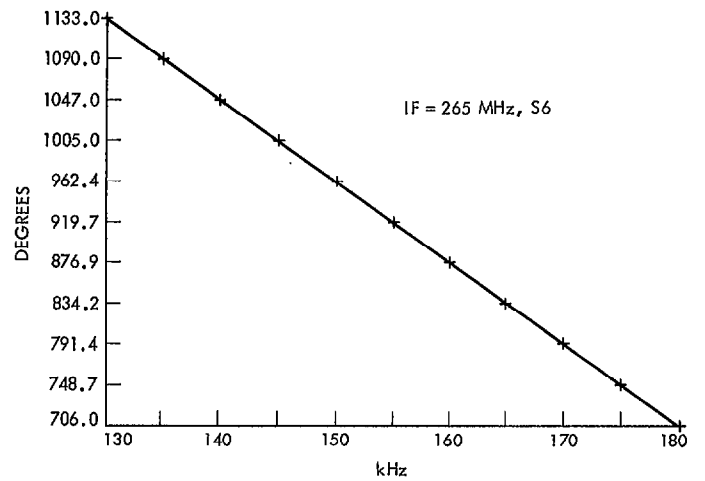
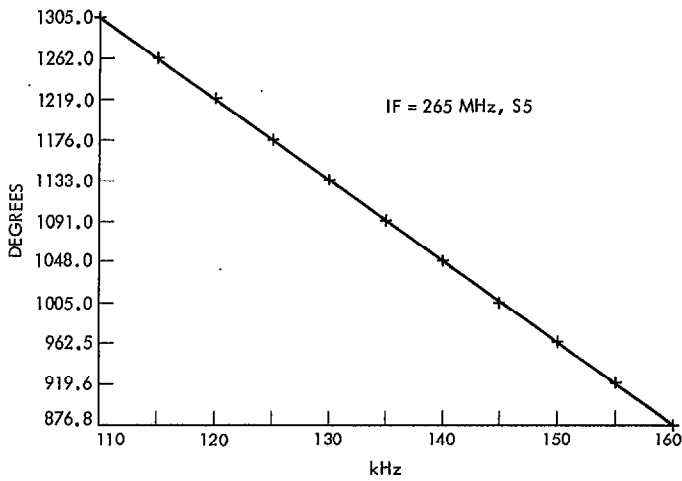


Fig. 14. Linear regression analysis results from 110 to 180 kHz

R SQUARE = 1.000

YHAT = 2265.253 + -8.668 X

X(I)	Y(I)	YHAT	RESIDUALS
160.00	876.80	878.37	-1.57
165.00	834.10	835.03	-0.93
170.00	791.60	791.69	-0.09
175.00	748.80	748.35	0.45
180.00	706.00	705.01	0.99
185.00	663.00	661.67	1.33
190.00	619.70	618.33	1.37
195.00	576.10	574.99	1.11
200.00	532.10	531.65	0.45
205.00	487.80	488.31	-0.51
210.00	442.40	444.97	-2.57

R SQUARE = 0.999

YHAT = 2361.363 + -9.163 X

X(I)	Y(I)	YHAT	RESIDUALS
180.00	706.00	711.94	-5.94
185.00	663.00	666.12	-3.12
190.00	619.70	620.31	-0.61
195.00	576.10	574.49	1.61
200.00	532.10	528.67	3.43
205.00	487.80	482.85	4.95
210.00	442.40	437.04	5.36
215.00	395.60	391.22	4.38
220.00	347.30	345.40	1.90
225.00	297.00	299.59	-2.59
230.00	244.40	253.77	-9.37

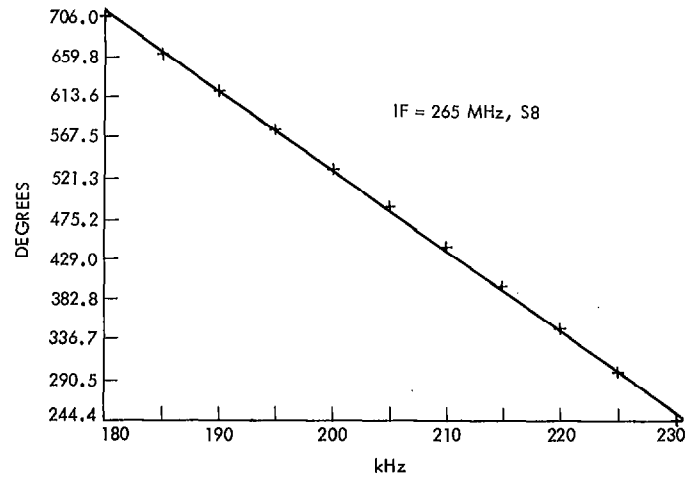
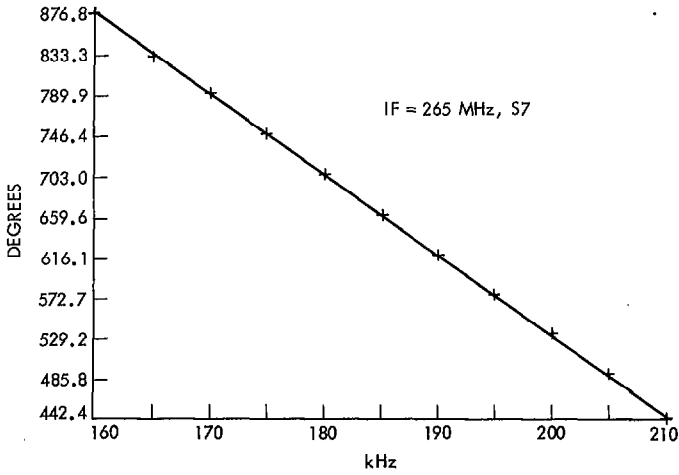


Fig. 15. Linear regression analysis results from 160 to 230 kHz